Rapid empirical battery electromotive-force and overpotential modelling using input-output linear parameter-varying methods

Journal of Energy Storage 65 (2023) 107185

Contents lists available at ScienceDirect

Journal of Energy Storage

journal homepage: www.elsevier.com/locate/est

Research papers

Rapid empirical battery electromotive-force and overpotential modelling using input–output linear parameter-varying methods

F.S.J. Hoekstra [a,*], M.C.F. Donkers [a], H.J. Bergveld [a,b]

[a] Department of Electrical Engineering, Eindhoven University of Technology, Groene Loper 19, 5612AP, Eindhoven, Netherlands
[b] NXP Semiconductors, High Tech Campus 46, 5656AE, Eindhoven, Netherlands

ARTICLE INFO

Keywords:
Battery modelling
Electromotive-force
Linear parameter-varying

ABSTRACT

In this paper, battery overpotential model identification approaches based on local and global Linear Parameter-Varying (LPV) input–output models are developed. Key features such as model structure, number of local models, and type and order of basis functions are considered. The LPVcore toolbox (Boef, 2021) has been used to solve the global identification problems. Furthermore, an iterative scheme is proposed which identifies a complete empirical battery model, i.e., both the ElectroMotive Force (EMF), also known as open-circuit voltage, and the overpotential model. This is achieved by iteratively obtaining an EMF realisation by (1) subtracting the modelled overpotential from a measured terminal voltage resulting from Constant-Current (CC) (dis)charging, and (2) using this EMF to calculate the overpotential from dynamic (dis)charging data and identifying an overpotential model using the LPV methods. This approach results in an empirical battery model with a precision similar (around 4 mV root-mean-square error in the range between 100% and 20% SoC) to models identified through a common cascaded approach in which the EMF is obtained separately from, e.g., pulse-(dis)charge data, but requires less measurement data resulting in a reduction factor in the order of 7 to 35 in terms of required experiment time.

1. Introduction

Li-ion batteries need to be closely monitored to use them safely and effectively. To do so, a Battery Management System (BMS) will measure the current, voltage and temperature of the battery at all times and will ensure that these indicators remain within safe boundaries [1]. Using the measurements quantities, the BMS does not only ensure safety, but also estimates internal information from the battery and make both long- and short-term predictions of several battery states using models which describe the relations between external measurements and internal processes or states. These models can generally be divided into electrochemical and empirical models, where the former focus on accurately describing internal battery processes which can for instance be used to minimise ageing, see, e.g., [2,3], and the latter excels at predicting the battery terminal voltage as a result of the applied current [4,5].

Due to their relative simplicity compared to electrochemical models, empirical models are currently the most commonly applied type of model in BMSs. Most popularly, they are known and used in the form of Equivalent-Circuit Models (ECMs), see, e.g., [5,6], where the battery behaviour is modelled by several linear [5], or nonlinear electrical components, to ensure accuracy over a wide range of frequencies [7]. However, for an application such as an electric vehicle, which exhibits primarily low-frequency behaviour, the inclusion of nonlinear elements may result in unnecessarily complicated models, while hardly contributing to its overall accuracy [7]. Instead, a more meaningful contribution is established by assuring model accuracy over a wide range of operating conditions. An additional benefit of empirical models is also that incorporating these dependencies is also readily possible. While a high level of accuracy can be attained by identifying an SoC- and temperature-dependent model, see, e.g., [8,9], it is not clear from literature how to do so in a consistent and concise manner, see, e.g., [4,5,7,9,10].

To better understand the available options in modelling such a linear, but external-variable- or state-dependent model, note that this type of model is known as a Linear Parameter-Varying (LPV) model [11], where the variable on which the behaviour depends is referred to as the scheduling variable. In terms of identification approaches, a distinction can be made between local and global methods. The local approach models the local system behaviour, i.e., at a fixed value of the scheduling variable, using well-known Linear Time-Invariant (LTI) system identification techniques. By repeating this for multiple values of the scheduling variable and by subsequently interpolating

* Corresponding author.
E-mail addresses: f.s.j.hoekstra@tue.nl (F.S.J. Hoekstra), m.c.f.donkers@tue.nl (M.C.F. Donkers), h.j.bergveld@tue.nl (H.J. Bergveld).

https://doi.org/10.1016/j.est.2023.107185
Received 4 July 2022; Received in revised form 18 January 2023; Accepted 16 March 2023
Available online 30 March 2023

between the obtained local models, one can describe the complete battery behaviour as a function of that particular scheduling variable. This is also a common approach in battery modelling, where model parameters are often said to be defined by lookup tables that describe certain dependencies, see, e.g., [7,10]. On the other hand, the global approach directly identifies the battery behaviour as a function of the scheduling variable. This is attractive in terms of modelling as it negates the effect of interpolating between local models and sometimes may even be necessary as it may be impossible to excite the battery without significantly changing the scheduling variable, see, e.g., [12]. In terms of global LPV identification methods, these can generally be split into Input–Output (IO) model-based approaches, see, e.g., [13], and State-Space (SS)-oriented approaches, see, e.g., [14,15]. The interest in modelling batteries using global LPV approaches has been limited, see, e.g., [16], where a general nonlinear optimisation approach was applied and [17,18] in which sub-space methods have been used, which is an LPV-SS method. To the authors' knowledge, LPV-IO methods have not been used before for modelling batteries, while these methods can be attractive from a computational point of view.

Besides the overpotential model, the empirical battery model also requires an ElectroMotive-Force (EMF) model, also known as open-circuit voltage. Typically, a cascaded identification approach is applied in which the EMF has been predetermined and can be subtracted from the terminal voltage, thus obtaining locally linear overpotential behaviour, which can be modelled using the aforementioned approaches. In these cases, the EMF has been determined through one of various methods, such as pulse-(dis)charge experiments or extra- or interpolation approaches, which rely on Constant-Current (CC) (dis)charge experiments. Although seemingly disjoint, these approaches still implicitly assume an overpotential model. For example, for pulsed experiments it is assumed that the overpotential is zero at some point after each pulse and for inter- and extrapolation-methods a polynomial overpotential function is assumed with respect to current. Instead of treating the modelling of the EMF and overpotential as two distinctly disjoint parts, it could also be possible to leverage this interaction to minimise the overall voltage prediction error of the model or to decrease the required experiment time, which is significant for the methods which are currently available [19].

In this paper, local and global IO-model-based LPV identification strategies are developed for empirically modelling the overpotential and an iterative scheme is proposed which identifies both the EMF and the overpotential model and requires only a limited amount of data. The LPV methods are applied for modelling the SoC dependency of the overpotential and the effect of different choices such as model structure, number of local models and type of basis functions is considered. By using accurate data and EMF realisations from [19], the best overpotential modelling strategy is determined for the classical disjoint EMF and overpotential modelling approach. Subsequently, these approaches are then used in the iterative scheme and the obtained results in terms of voltage prediction and SoC estimation error of the complete model are compared to those achieved in [19].

The outline of this paper is as follows. In Section 2, LPV model identification approaches are discussed for modelling general overpotential dependencies. In Section 3, the iterative scheme is proposed and its boundary conditions are discussed. In Section 4, modelling results for both the separate overpotential modelling and the iterative method are presented. Finally, conclusions are drawn in Section 5.

2. Linear parameter-varying overpotential modelling

The battery model assumed in this paper is given by

$$\hat{y}_k = g(s_k) + h(\boldsymbol{p}_k, \boldsymbol{u}_k, \Theta) \tag{1}$$

with time $k \in \mathbb{N}$, the predicted terminal voltage $\hat{y}_k$ with the hat indicating prediction, the Electromotive-Force (EMF) $g(s_k)$, the SoC s_k given by

$$s_k = s_0 + \sum_{i=0}^{k} \frac{\tau u_i}{C_0}, \tag{2}$$

with C_0 [As] the cell capacity, u_k the model input, which is the current applied to the battery and τ is the model sampling time. Furthermore, $h(\boldsymbol{p}_k, \boldsymbol{u}_k, \Theta)$ is the overpotential model with $\boldsymbol{p}_k = \{p_0, \dots, p_k\}$ the collection of one or multiple scheduling variables of the current and past time instances making (1) a Linear Parameter-Varying (LPV) model, $\boldsymbol{u}_k = \{u_0, \dots, u_k\}$ is the collection of model inputs, and Θ the set of model parameters. A common choice for $h(\boldsymbol{p}_k, \boldsymbol{u}_k, \Theta)$ is to make it a solution of a difference equation in the shape of an SS model, as given by

$$o_{k+1} = \begin{bmatrix} \theta_{1,1}(p_k) & \cdots & 0 \\ \vdots & \ddots & \vdots \\ 0 & \cdots & \theta_{1,N}(p_k) \end{bmatrix} o_k + \begin{bmatrix} \theta_{2,1}(p_k) \\ \vdots \\ \theta_{2,N}(p_k) \end{bmatrix} u_k, \tag{3a}$$

$$\hat{y}^o_k = C o_k + \theta_3(p_k) u_k, \tag{3b}$$

with $o_k \in \mathbb{R}^{N\times 1}$ the dynamic part of the overpotential with N the system order, $\hat{y}^o_k$ the total predicted overpotential, $\theta_{1,i}(p_k)$ with $i \in \{1, \dots, N\}$ the overpotential relaxation rate, $\theta_{2,i}(p_k)$ the overpotential increase due to applied current, $C = [1, \dots, 1] \in \mathbb{R}^{1\times N}$ and $\theta_3(p_k)$ which represents the Ohmic resistance and all high-frequency impedances, i.e., higher than the model sampling frequency. The applied model is the same as an ECM, but without transforming the parameters to R and C values, see, e.g., [20], for details on their equivalence. In this paper, it is assumed that the model order $N = 1$, such that (3) is a first-order model with $\theta_{1,1} = \theta_1$ and $\theta_{2,1} = \theta_2$. However, note that the presented methods are also valid for higher-order systems. The choice for $N = 1$ is often considered sufficient, as was demonstrated in [21].

The battery overpotential model (3) is presented in State-Space (SS) form, as this is also the representation used for common battery model applications such as state estimation or model-predictive control. Identifying the LPV overpotential model can be done using a broad range of approaches, see [11] for an overview. Typically, these approaches either rely on LPV-SS or LPV-IO model representations, which in turn are associated with different identification algorithms. For instance, for LPV-SS modelling there are gradient-based methods, see, e.g., [14], but also subspace-based methods, see, e.g., [15]. On the other hand, for IO representations there are linear-regression-based approaches, see, e.g., [22], which are computationally attractive. The need for direct identification of LPV-SS models is often motivated from a control perspective, as most LPV control-design strategies are based on SS models, see, e.g., [23]. Besides this, the use of direct-SS approaches can be desired if a specific SS model structure needs to be preserved, for instance in grey-box modelling, which is similar to the motivation for LTI SS models [24].

For electrical modelling of batteries, the focus is often on accurate modelling of the battery terminal voltage, where no specific model structure or knowledge on the internal state is desired. This allows the use of black-box modelling, specifically the use of IO-based approaches. Due to its computational benefits, the focus of this paper will be on model identification using IO-based representations. The general LPV-IO model equivalent of the overpotential SS model in (3) is given by

$$A(q, p_k) y^o_k = \frac{B(q, p_k)}{F(q, p_k)} u_k + e_k \tag{4}$$

where q is the shift operator, i.e., $q^{-1} x_k = x_{k-1}$, e_k is the noise and the 'measured' overpotential y^o_k given by

$$y^o_k = y_k - g(s_k), \tag{5}$$

where y_k is the measured terminal voltage.

2.1. IO model structures

The exact realisation of (4) depends on the selected model structure, i.e., which noise model is applied. In this paper, two specific structures are considered, namely AutoRegressive with eXogenous input (ARX), which is given by

$$A(q,p) = 1 + a_1(q^{-1}p)\,q^{-1}, \quad F(q,p) = 1,$$
$$B(q,p) = b_0(p) + b_1(q^{-1}p)\,q^{-1}, \tag{6}$$

and secondly, Output-Error (OE), which is given by

$$A(q,p) = 1, \quad F(q,p) = 1 + f_1(q^{-1}p)\,q^{-1},$$
$$B(q,p) = b_0(p) + b_1(q^{-1}p)\,q^{-1}. \tag{7}$$

In (6) and (7), the parameters depend dynamically on p, i.e., the time-shifted version of p. This ensures that the IO parameters map to SS parameters according to

$$\theta_1(p) = -a_1(p), \quad \theta_2(p) = b_1(p) - a_1(p)b_0(p), \quad \theta_3(p) = b_0(p), \tag{8}$$

and

$$\theta_1(p) = -f_1(p), \quad \theta_2(p) = b_1(p) - f_1(p)b_0(p), \quad \theta_3(p) = b_0(p), \tag{9}$$

for ARX and OE, respectively, where θ_1, θ_2 and θ_3 only depend on p as in (3), and not the shifted version of p, i.e., $q^{-1}p$, see [25] for the derivation. Assuming a static dependency on p in (4) and ignoring the consequent dynamic dependency after transformation to SS leads to an approximation error, as explained in [25]. For batteries, this error is small as long as the model sampling time is relatively low with respect to the slow changing scheduling variables, such as SoC or temperature.

While these models share the same plant model, they differentiate themselves through the way that they deal with the presence of noise. In case of battery modelling, which is a complex electrochemical system, noise should be interpreted as all parts of the behaviour of the battery which cannot be captured by (4) and thus represents unmodelled dynamics. There are two consequences to this observation with respect to which model structure would be most suitable for modelling battery behaviour. First, we should consider the nature of that part of the behaviour of the battery that cannot be captured, i.e., the nature of the noise. Second, as the models can only describe a part of the full battery dynamics, their approximate modelling characteristics need to be considered.

Let us first consider the battery behaviour that cannot be modelled. When modelling the overpotential $\hat{y}^o$, one should recognise that an SoC-dependent offset can occur through the use of an incorrect EMF $g(s_k)$, as can be deduced from (5). As shown in [19], the validity of the applied realisation $g(s_k)$ has a large impact on the overall model accuracy. These errors are most pronounced in the relaxation behaviour of the overpotential, which is modelled by A or F in (4). With respect to the choice of type of IO model, the reasoning is that the behaviour of the model errors is similar to that of the relaxation of the battery. Hence, ARX, where the noise model is given by $\frac{1}{A(q,p)}$, is deemed to be more suitable compared to OE, whose noise model equals 1 and thus assumes that the output is directly affected by white noise.

Secondly, when applying the Prediction-Error Minimisation (PEM) framework to identify models, see [24], which cannot fully describe the true system, also known as approximate modelling, it is known that ARX and OE have a different modelling focus. Since the noise model for OE equals 1, this means that all frequencies are weighed equally. However, the noise model of the ARX structure results in a high-pass filter, thus emphasising the high-frequency content of the model. Remembering that most errors are likely to be in the relaxation behaviour, which is low-frequency, it could be that OE is more susceptible to this type of error. On the other hand, low-frequency behaviour does have a dominant share in the prediction error. Thus, if the EMF is correct, OE could potentially focus more strongly on the low-frequency behaviour, thus resulting in a lower prediction error.

2.2. Local approach

In terms of the parametrisation of (4), one can use either the local or the global modelling approach, as discussed in the introduction. For a comprehensive overview of both of these methods for the case of IO models, see [13]. The local approach relies on the principle that if the scheduling variable of the system is (approximately) constant while the system is excited, then its behaviour can be modelled as LTI. By repeating this for different values of the scheduling variable, multiple LTI models can be identified which together represent the system behaviour over the whole range of the scheduling variable. From an experimental perspective, this can mean that the battery is excited at distinct operating points, for example at different temperatures. However, it is also possible to apply continuous excitation while the scheduling variable changes slowly. By dividing this data into several segments, where the change in scheduling variable is minor within each segment, it is also possible to approximate the behaviour at each piece using an LTI model.

More formally, for total data length K, we can have individual data segments $\mathcal{K}_m = \{K_{m-1}, \dots, K_m - 1\}$ with $K_{m-1} < K_m$, $K_0 = 0$, $K_M = K$, and $m = \{1, \dots, M\}$ is the interval number with M the total number of intervals. Subsequently, at each local data set we consider the one-step-ahead predictor $\hat{y}^o_{k|k-1}$, see [24] for the derivation, given by

$$\hat{y}^o_{k|k-1} = \frac{B_m(q)}{F_m(q)}u_k + \Big(1 - A_m(q)\Big)y^o_k, \tag{10}$$

whose parameters $\Theta_m = (a_{1,m}, f_{1,m}, b_{0,m}, b_{1,m})$ are estimated by solving the least-squares problem

$$\min_{\Theta_m} \quad \sum_{k\in\mathcal{K}_m} \left(y^o_k - \hat{y}^o_{k|k-1}\right)^2, \tag{11}$$

which can be solved using LTI system identification techniques. By solving (11) subject to (10) for each interval of the experimental data $\mathcal{K}_m$, a collection of local models is obtained. The remaining step is to link these models to their corresponding value of the scheduling variable, thus obtaining a set of p-dependent parameters. Therefore, the average value of p of the corresponding interval, given by

$$\bar{p}_m = \tfrac{1}{K_m - K_{m-1}} \sum_{k\in\mathcal{K}_m} p_k, \tag{12}$$

where $K_m - K_{m-1}$ is the number of elements of set $\mathcal{K}^m$, is assigned to each set of parameters Θ_m, thus describing the complete parameter set $\Theta = (\Theta_1, \dots, \Theta_M)$ over p. The transformation of the ARX structure to SS parameters used in (3), is given by

$$\theta_1(p) = \{-a_{1,1}, \dots, -a_{1,M}\},$$
$$\theta_2(p) = \{(b_{1,1} - a_{1,1}b_{0,1}), \dots, (b_{1,M} - a_{1,M}b_{0,M})\}, \tag{13}$$
$$\theta_3(p) = \{b_{0,1}, \dots, b_{0,M}\},$$

where substituting $a_{1,m}$ with $f_{1,m}$ yields the SS parameters for the OE structure. The values in between the scheduling points are found by interpolating between the local LTI models with respect to the scheduling variable. Alternatively, one could also interpolate the inputs or outputs of the different LTI models, but for batteries the common choice is to interpolate the model parameters. Note that $M = 1$ yields an LTI model and is thus omitted from the interval options. A benefit of the local approach is that (11) can be solved using well-known LTI system identification techniques, which for an ARX model structure yields a convex optimisation problem that can be solved analytically, and for OE, which results in a non-convex problem, well-known gradient or subspace-based methods can be applied.

2.3. Global approach

A drawback to the local approach is that this method, depending on the system or type of scheduling variable, may not always be feasible. For instance, if the scheduling variable is also a system state, it may not be possible to excite the system without significantly changing the scheduling variable. In that case, the global approach provides a good alternative, as it estimates the parametric dependency of the model based on a single data set in which the scheduling variable changes continuously. For the global approach, we consider the one-step-ahead predictor $\hat{y}^o_{k|k-1}$, similar to (10), given by

$$\hat{y}^o_{k|k-1} = \frac{B(q,p_k)}{F(q,p_k)}u_k + \Big(1 - A(q,p_k)\Big)y^o_k, \tag{14}$$

with $A(q,p_k)$, $F(q,p_k)$ and $B(q,p_k)$ according to (6) or (7), where its corresponding parameters are estimated by

$$\min_{\Theta} \quad \sum_{k\in\mathcal{K}} \Big(y^o_k - \hat{y}^o_{k|k-1}\Big)^2, \tag{15}$$

subject to (14), with $\Theta = \Big(a_1(q^{-1}p), f_1(q^{-1}p), b_0(p), b_1(q^{-1}p)\Big)$ the parameters obtained via the global approach and where $\mathcal{K} = \{0,\dots,K\}$ denotes the complete data set in which p changes dynamically. Opposed to the local problem (11), solving (15) is not trivial. In this paper, the LPVcore toolbox of [26] is used to solve the global identification problem, which in turn applies the approach of [22].

For the global approach, one is required to select basis functions which describe the structure of the dependency of the parameters $a_1(q^{-1}p)$, $f_1(q^{-1}p)$, $b_0(p)$ and $b_1(q^{-1}p)$ on the scheduling variable p_k. For most global modelling algorithms to work, the basis function should be linear-in-the-parameters [13]. Therefore, a common choice is to assume that the parameters have a polynomial dependency, according to

$$\Big(a_1(q^{-1}p), f_1(q^{-1}p), b_0(p), b_1(q^{-1}p)\Big) = \sum_{n=0}^{N} \phi_n p^n, \tag{16}$$

with the polynomial index $n = \{0,\dots,N\}$ with N the polynomial order and ϕ_n its free parameters. While this does not require any knowledge on the model dependency, it may not be an efficient parametrisation because relatively high-order polynomials could be required to accurately describe the dynamics. For batteries, it is also been successful to apply exponential basis functions

$$\Big(a_1(q^{-1}p), f_1(q^{-1}p), b_0(p), b_1(q^{-1}p)\Big) = \phi_0 + \phi_1 e^{\beta s}, \tag{17}$$

for modelling the SoC dependency [27] or temperature dependency [12]. Determining whether or not a basis function is suitable can readily be done by first applying the local approach to see what the general trend of the dependency looks like. In case of modelling the temperature dependency, one can also reason from a physics-informed point of view/use a grey-box approach. Namely, a battery is an electrochemical system and its internal processes are temperature-dependent according to an Arrhenius (exponential) type of relation and hence exponential basis functions (17) could be effective. The only caveat here is that β in (17) is not an linear parameter, and therefore it must be estimated a priori. In practice, this can be done by fitting the exponential relation on a number of local realisations of the model, as will be shown in Section 4. Overall, the exponential basis functions can reduce the number of parameters, while increasing or maintaining the accuracy of the model, as will also be shown in Section 4.

3. Iterative complete battery model identification

In Section 2, a model of the EMF $g(s_k)$ is required to model the overpotential behaviour $h(\boldsymbol{p}_k, \boldsymbol{u}_k, \Theta)$. As discussed in [19], the identification of an accurate $g(s_k)$ through conventional approaches is time-consuming, while also modelling the EMF typically requires some model of the overpotential. In this paper, we propose to set aside the decoupled modelling strategy, in which first the EMF is identified and subsequently the overpotential model. This leads to a speedup, as leveraging this relationship allows us to use data which requires less experiment time. Therefore, we propose a direct identification of the complete battery model, as given by

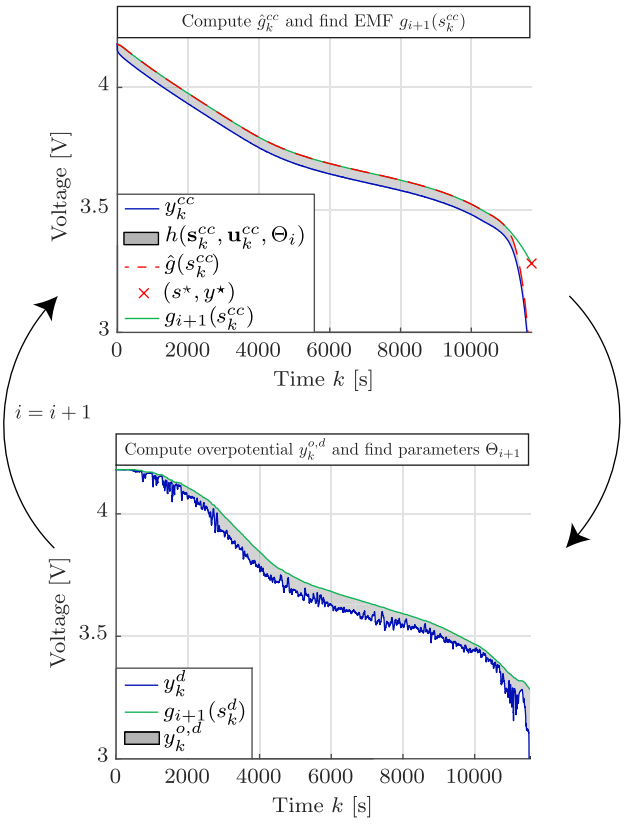

Fig. 1. Illustration of the iterative modelling approach, with $\hat{g}(s_k^{cc}) = y_k^{ss} - h(\boldsymbol{s}_k^{cc}, \boldsymbol{u}_k^{cc}, \Theta_i)$ and $y_k^{o,d} = y_k^d - g_{i+1}(s_k^d)$, as given in Step 3.3 and 4.3 of the algorithm, respectively.

$$\min_{g(s_k),\Theta} \quad \sum_{k\in\mathcal{K}} \Big(y_k - g(s_k) - h(\boldsymbol{p}_k, \boldsymbol{u}_k, \Theta)\Big)^2. \tag{18}$$

Problem (18) is hard to solve due to the large degree of freedom that the combination of $g(s_k)$ and $h(\boldsymbol{p}_k, \boldsymbol{u}_k, \Theta)$ gives. For this reason, it cannot be readily solved using standard nonlinear optimisation algorithms, as for instance attempted in [16].

To understand the approach that will be proposed in this section, let us first briefly consider the hypothetical case in which the overpotential model parameters Θ are known, but the EMF model $g(s_k)$ is not. The EMF could be determined by simply reversing the order of (5), such that we have

$$g(s_k) = y_k - h(\boldsymbol{p}_k, \boldsymbol{u}_k, \Theta), \tag{19}$$

where y_k could be any terminal voltage measurement where the corresponding current $\boldsymbol{u}_k$ should establish a significant coverage of the domain of s_k according to (2), i.e., the SoC on which the EMF depends. By considering (19), (5) and either (11) or (15) in an iterative fashion, one can come to successive estimates of $g(s_k)$ and Θ. Based on this principle, we propose the iterative identification scheme as provided by Algorithm 1, where we update the EMF model based on the overpotential model (Step 3.3) and subsequently update the overpotential model based on the improved EMF model (Step 4.4). A schematic representation of this is shown in Fig. 1. Due to the primary dependency of $g(s_k)$ on the SoC, it is vital that p_k in $h(\boldsymbol{p}_k, \boldsymbol{u}_k, \Theta)$ at least includes SoC. For clarity, we will denote $\boldsymbol{p}_k = \boldsymbol{s}_k$, with s_k according to (2).

This approach requires the selection of an initial guess of the overpotential model Θ_0 which can be a simple LTI model to start off, step size $\alpha \in (0, 1]$ which controls the convergence rate, with $\alpha = 1$ constituting a full step, i.e., direct adaptation of a new estimate, and $\alpha < 1$ a blend with previous estimates, and termination criterion ϵ. In order to obtain meaningful results using this approach and to solve Problem (18), we first consider the applied data on which the model is identified. Two different measurements of y_k are used in Steps 3.3 and 4.3, namely Constant-Current (CC) (dis)charge, denoted by superscript cc, and dynamic (dis)charge data, denoted by superscript d, respectively. These data sets are associated with SoC windows s_k^{cc} and s_k^d, respectively. The resulting $g(s_k)$ has SoC range $s_{k\in\mathcal{K}} \in \mathcal{S} = [\min(\{s^{cc}_{k\in\mathcal{K}}\} \cap \{s^d_{k\in\mathcal{K}}\}), \max(\{s^{cc}_{k\in\mathcal{K}}\} \cap \{s^d_{k\in\mathcal{K}}\})]$. The use of CC (dis)charge data is important as this results in a smooth and often monotone realisation of $y_k^{cc} - h(\boldsymbol{s}_k^{cc}, \boldsymbol{u}_k^{cc}, \Theta)$, thus simplifying Step 3.4 of the algorithm. On the other hand, the dynamic (dis)charge cycle is required to sufficiently excite the dynamics of the overpotential, which is critical for correctly estimating Θ_{i+1}.

Besides selecting the data, we also restrict the freedom in $g(s_k)$ to limit susceptibility to overfitting. Three constraints are imposed on the initial realisation of $g(s_k)$ obtained through (19), namely:

1. An upper- or lower-bound is imposed on the EMF, according to $g(s^\star) = y^\star$, with $y^\star$ a relaxed terminal voltage at SoC-point $s^\star = \max(\{s^{cc}_{k\in\mathcal{K}}\} \cap \{s^d_{k\in\mathcal{K}}\})$ after charging or $s^\star = \min(\{s^{cc}_{k\in\mathcal{K}}\} \cap \{s^d_{k\in\mathcal{K}}\})$ after discharging, respectively. The voltage bound $y^\star$ is given by the relaxed voltage after (dis)charging corresponding to the data with the most restrictive SoC window. In the top window of Fig. 1, it is shown how a point $(s^\star, y^\star)$ is used as a lower bound for a discharging EMF.
2. $g(s_k)$ must be a monotonically increasing function of SoC, i.e., $g(s_1) < g(s_2)$ for all $s_1 < s_2$.
3. The enforced upper- or lower-bound must preserve the shape of the EMF according to

$$\frac{g(s_j) - y^\star}{s_j - s^\star} \geq \frac{g(s_{j+1}) - g(s_j)}{s_{j+1} - s_j}, \tag{20}$$

for discharging and

$$\frac{y^\star - g(s_{J-j})}{s^\star - s_{J-j}} \geq \frac{g(s_{J-j}) - g(s_{J-j-1})}{s_{J-j} - s_{J-j-1}}, \tag{21}$$

for charging, where J is the maximum number of partitions of $g(s)$. Enforcing the constraints is done by simply stepping from $j = 1$ to J, until (20) or (21) is satisfied after which $g(s) = \{y^\star\ g(s_j), \dots, g(s_J)\}$ or $g(s) = \{g(s_1), \dots, g(s_{J-j})\ y^\star\}$, for discharging and charging, respectively. In the top window of Fig. 1, the part of the green line ($g_{i+1}(s_k^{cc})$ connecting $(s^\star, y^\star)$ and the dashed red line is the result of forcing monotonicity on the gradient according to (21).

Lastly, note that the absolute values of the SoC range underpinning the obtained model are somewhat arbitrary, i.e., as long as g and h are characterised with respect to the same frame of reference, which is ensured by choosing s_1^d based on g in Step 4.2, the model produces accurate voltage predictions, no matter what the selected initial SoC s_1^{cc} in Step 3.2 is. However, to operate within the commonly accepted frame of reference that $s = 1$ equals fully charged, we can set $s_1^{cc} = 1$ for CC-discharge curves, thus assuming a fully charged condition before commencing discharging. For CC-charging, it is possible to track the level of discharging that occurred before the CC-charging started. If this discharging commenced from a fully charged condition, i.e., $s = 1$, one can simply track the SoC using (2) and assume that the final SoC equals s_1^{cc}. If g and h need to be characterised for both charging and discharging, one can align these models by assuming that, e.g., a Constant-Current Constant-Voltage (CCCV) charge leads-to a fully charged condition, i.e., $s = 1$.

Algorithm 1: Iterative modelling approach

Input: Θ_0, α, ϵ, y_k^{cc}, u_k^{cc}, y_k^d, u_k^d
Output: $g(s_k), \Theta$

1 $i = 0$
2 **repeat**
3.1 **Identification of** g
3.2 Compute s_k^{cc} according to (2) with $s_1^{cc} \in [0, 1]$
3.3 Approximate EMF:
$$\hat{g}(s) = y_k^{cc} - h(\boldsymbol{s}_k^{cc}, \boldsymbol{u}_k^{cc}, \Theta_i)$$
3.4 Set upper- or lower-bound $g(s^\star) = y^\star$, and ensure monotonicity of $g(s)$ for all $s \in \mathcal{S}$ and $\nabla_s g(s)$ near $s^\star$ using (20) or (21).
3.5 Compute step:
if $i = 0$, $g_{i+1}(s) = \hat{g}(s)$
else $g_{i+1}(s) = \alpha\hat{g}(s) + (1 - \alpha)g_i(s)$
4.1 **Identification of** h
4.2 Compute s_k^d according to (2) with s_1^d such that $y_k^d = g_{i+1}(s_1^d)$
4.3 Compute dynamical overpotential:
$$y_k^{o,d} = y_k^d - g_{i+1}(s_k^d)$$
4.4 Identify overpotential model using (15):
$$\Theta_{i+1} = \underset{\Theta_{i+1}}{\operatorname{argmin}} \sum_{k\in\mathcal{K}_d} \left(y_k^{o,d} - h(\boldsymbol{s}_k^d, \boldsymbol{u}_k^d, \Theta_{i+1})\right)^2$$
5 Compute error with h a solution to (4):
$$e_i = \sum_{k\in\mathcal{K}_d} \left(y_k^d - g(s_k^d) - h(\boldsymbol{s}_k^d, \boldsymbol{u}_k^d, \Theta_{i+1})\right)^2$$
6 **until** $|e_{i+1} - e_i| < \epsilon$

4. Results

In this section, the performance of both local and global LPV modelling approaches discussed in Section 2, and the iterative algorithm proposed in Section 3, will be considered. In this paper, we only consider SoC dependency for the overpotential model, i.e., $p = s$, as this is crucial for the iterative algorithm where the EMF primarily depends on SoC. Although other dependencies have not been explored, it is assumed that extension to, e.g., temperature can be readily made, albeit with different basis functions or polynomial orders. The data used in this paper is the same as in [19], measured on two cells, namely one Lithium Nickel-Manganese-Cobalt (NMC) cell and one Lithium-iron-Phosphate (LFP) cell. The data consists of pulse-charge and -discharge experiments, CC-charge and -discharge curves at C-rates {0.05, 0.1, 0.15, 0.2, 0.3, 0.5} and various drive cycles. An impression of the applied data is given in Fig. 2, which shows the discharge cycle used to identify the discharge overpotential models for NMC and LFP. For the full data, the reader is referred to Fig. 4.2 in [19].

4.1. Comparison of local and global LPV approaches

For the comparison of the local and global LPV overpotential modelling approaches, the following setting has been considered. First of all, for brevity, we have only considered the discharging case for this comparison. From [19], we have found that this is the most challenging, as the most significant SoC dependency of the overpotential model is encountered during discharging. Different from Section 3, we have

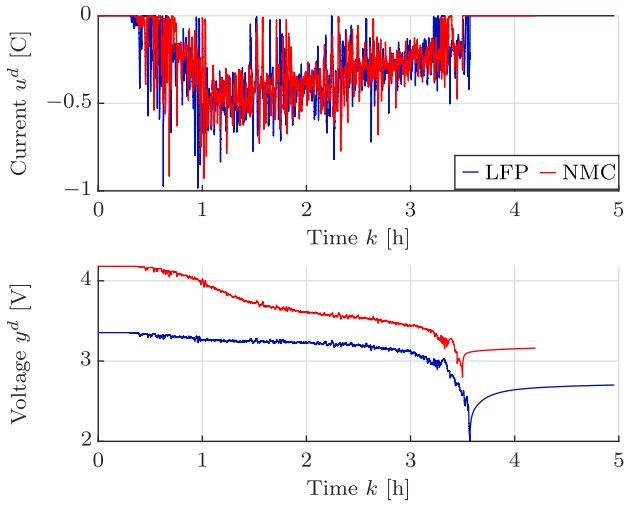

Fig. 2. Dynamic discharge data used to identify the overpotential models. Both the dynamic identification and validation cycles are based on drive cycles, which are suitable as they excite the battery over a wide frequency range, for more details see, e.g., [28].

first assumed the classical approach in which $g(s)$ has been obtained up-front. In this case, two realisations from [19] have been applied, namely one obtained using the extrapolation-based method (EMF_1), and secondly an EMF realisation corresponding to the pulse-discharge experiment (EMF_2), with 56 and 62 relaxation points for NMC and LFP, respectively. Results in [19] showed that EMF_1 yields the most accurate results. For the local approach we have considered the number of local models $M = \{10, 15, \dots, 60\}$ in intervals of 5 and for the global approach we have used polynomial dependency according to (16) with order $N = \{4, \dots, 10\}$.

The overpotential models have been identified on one discharging drive cycle with time steps $k \in \mathcal{K}$ and have been validated on a second drive cycle. To validate the performance of the IO overpotential models, where the reader should recall that the current is the input and the overpotential voltage the output, we evaluate (18), where the EMF $g(s_k)$ remains equal but different realisation of $h(\boldsymbol{p}_k, \boldsymbol{u}_k, \Theta)$ are evaluated. This means that the error between the measured and predicted overpotential, i.e., y_k^o and $\hat{y}_k^o$, is evaluated. Specifically, the Root-Mean-Square Error (RMSE) is considered, as this is the error term which is also minimised by the PEM framework. The validation results reported as RMSE are shown in Fig. 3. In this figure, the upper 6 subfigures are NMC and the lower 6 are LFP, and show the results for the local and global approach. Errors on both the full range, i.e., for the complete drive cycle, and the limited range, i.e., excluding the last 1% and 9% that have been removed for NMC and LFP, respectively, are considered. In these last parts, where the EMF is steepest, most of the errors occur and this can thus obscure the model performance over the largest portion of the battery operating range. The exclusion percentage is larger for LFP due to its relatively large steep section of the EMF. There are two likely causes of the increase in error. First of all, when the EMF is steep, any errors in the EMF model quickly produce relatively large errors in terms of predicted voltage. Secondly, at low SoC some parts of the overpotential are weakly nonlinear [29]. This means that the linear structure of (4) will not be able to describe all the behaviour.

Let us first consider the results for the local approach in Figs. 3(a) and 3(d). It is observed that for SoC dependency this approach yields consistent results if the number of local models is sufficiently large ($M \geq 40$), i.e., the full-range errors remain approximately the same, where the limited-range errors continue to drop slightly. This approach does not provide consistent results for $M < 40$, where especially OE models produce erratic results. Overall, the local approach does establish the lowest RMSE for the limited range, when compared to the global approach. Secondly, the results for the global approach using polynomial basis functions are considered, as shown in Figs. 3(b) and 3(e). In this case, the influence of the polynomial order is much stronger for the NMC cell, which has RMSEs above 75 mV for $N = 4$ and $N = 10$ for the full range, whereas the LFP cell attains decent performance for almost all polynomial orders. However, also here, an error increase is observed for $N > 6$. On the other hand, the error keeps decreasing for the limited range, which is similar to the local approach. This shows that a large degree of freedom is required to accurately model the overpotential dynamics over the limited range, whereas too much freedom results in higher errors for the full range. Optimal performance is attained for $N = 6$ and $N = 7$ for the NMC cell, and for $N = 5$ and $N = 6$ for the LFP cell.

Instead of using purely polynomial basis functions for the global approach, which, as Figs. 3(b) and 3(e) show, can be sensitive to the applied polynomial order, we also apply the exponential basis functions proposed in Section 2.3. However, let us consider the parametric dependency of $\theta_1(s)$, $\theta_2(s)$ and $\theta_3(s)$, identified using the local and global approach, with 6th-order polynomial basis functions, for the NMC cell in Fig. 4. A strong resemblance for these two approaches can be observed for $\theta_2(s)$ and $\theta_3(s)$, while the difference on $\theta_1(s)$ is much larger. In this case, an exponential basis function is employed only for θ_1 as given by

$$a_1(s) = \phi_0 + \phi_1 e^{\beta s} \text{ or } f_1(s) = \phi_0 + \phi_1 e^{\beta s}, \tag{22}$$

where ϕ_0 and ϕ_1 are linear parameters and β, which dictates the curvature of the exponent, is predetermined using the local approach. While the resulting dependency in Fig. 4 is close to linear, it can occur that $\theta_1(s)$ sharply increases or decreases at low SoC, as for instance encountered in [27]. The benefit of this parametrisation is that the amount of freedom in $\theta_1(s)$, which describes the overpotential relaxation behaviour, is restricted. Since errors in the relaxation behaviour are strongly linked to errors in the EMF, as described in Section 2.1, restricting freedom in $\theta_1(s)$ can prevent overfitting. Meanwhile, by keeping $\theta_2(s)$ and $\theta_3(s)$ as polynomial functions, we do allow enough freedom to capture subtle differences in impedance at higher SoC. The corresponding RMSEs of this parametrisation in Figs. 3(c) and 3(f) show that the exponential parametrisation of $\theta_1(s)$ results in higher errors on average, as is expected when restricting freedom, but does yield a wider range of acceptable polynomial orders.

Lastly, the performance difference between ARX and OE is considered. The most notable difference between the two occurs for the local approach at $M < 40$, where OE either establishes poor performance, as observed for the NMC cell, or highly variable performance for the LFP cell, depending the exact EMF realisation. The difference with ARX could be explained by the frequency content of the data partitions used to identify the local models in (11), i.e., as the number of local models becomes smaller, the data length per partition $\mathcal{K}^m$ increases. As a result, the magnitude of low-frequency behaviour becomes relatively dominant and the OE model mainly captures this behaviour. However, due to the high-frequency focus of the ARX structure explained in Section 2.1, it maintains a stable trend as M increases.

4.2. Iterative battery model identification

Let us now discuss the performance of the iterative algorithm proposed in Section 3. First of all, note that in this case both the charging model and the discharging model are identified, where CC charging or discharging data paired with charging or discharging drive cycles, result in models valid for charging or discharging, respectively. In terms of inputs, the measured CC-charge and -discharge curves are used for u_k^{cc} and y_k^{cc}, and the overpotential model is identified on the drive-cycle charge- and discharge-data, the latter of which is the same as applied for identification in the previous section. The initial LTI model M_0 is selected to be $\theta_1 = 0.98$, $\theta_2 = 6 \cdot 10^{-4}$ and $\theta_3 = 0.035$, where

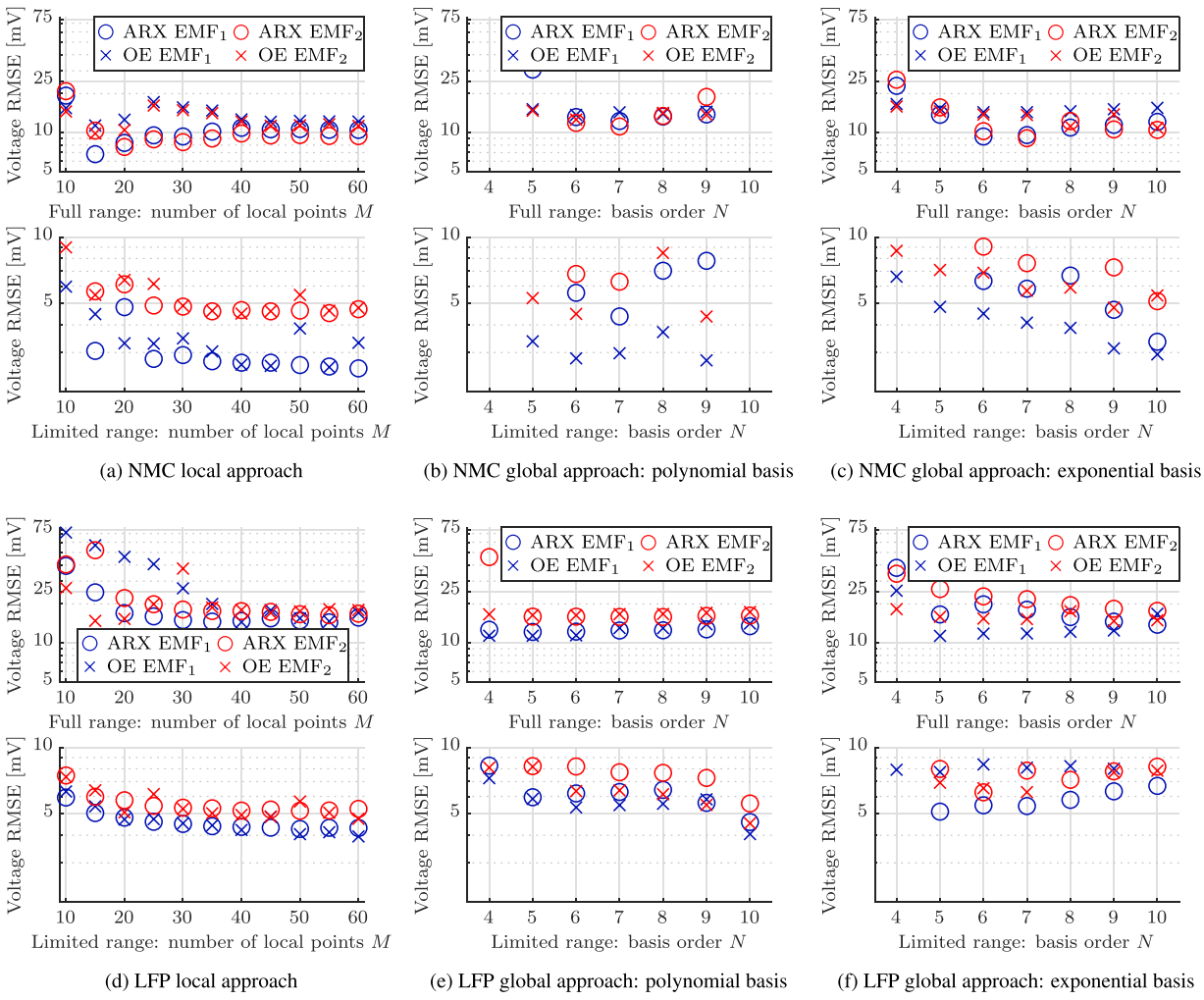

(a) NMC local approach (b) NMC global approach: polynomial basis (c) NMC global approach: exponential basis

(d) LFP local approach (e) LFP global approach: polynomial basis (f) LFP global approach: exponential basis

Fig. 3. Voltage RMSE for the validation drive cycle.

especially θ_1 and θ_2 are typical values for a battery model and where θ_3, which models all rapid impedances for times below the model sampling time and also the Ohmic resistance, differs more strongly per cell form factor or chemistry. However, these values are used as initial model for both the NMC and the LFP cell, so exact knowledge of the model is not required. Furthermore, termination criterion $\epsilon = 0.1$mV, and step size $\alpha = 1$ for the NMC cell and $\alpha = 0.5$ for the LFP cell, which is necessary to ensure convergence for the flat EMF corresponding to this chemistry. To solve Step 4.4 of the algorithm, the global approach with ARX model structure is employed. In case of a poor EMF, it is likely that poor local models are identified using the local approach, which again motivates the use of the global approach. ARX is employed because the performance difference with OE was found to be small in Section 4.1, but the algorithm used to identify it is more reliable, especially when the EMF is poor. It is also faster, which is convenient when multiple iterations are done.

In order to quantitatively judge the performance of various retrieved battery model realisations, we propose to consider both voltage prediction and SoC estimation accuracy in this paper, as in [19]. While the link between voltage prediction accuracy and performance of the battery model is clear, which now comes down to evaluating (18) for different realisations of both $g(s_k)$ and $h(\boldsymbol{p}_k, \boldsymbol{u}_k, \boldsymbol{\Theta})$, the necessity for evaluating SoC estimation performance is less obvious. Before motivating this further, let us first note that evaluating the battery model performance, and in particular the quality of retrieved EMF, based on SoC estimation accuracy only makes sense when a model-based approach is applied, i.e., when the model is actually involved in the estimation process. The reason why SoC estimation is interesting is that many model-based approaches, such as a Kalman Filter, see, e.g., [30] for details, depend on derivatives of the different model components with respect to the SoC. Having pronounced derivatives becomes especially important when the EMF is very flat, as, e.g., encountered with LFP or Lithium-Titanate-Oxide chemistries. In that sense, SoC estimation highlights a different aspect of the battery models. However, one should always consider a combination of voltage prediction and SoC estimation accuracy, as tuning of the SoC estimation algorithm can influence which part of the model is highlighted.

For SoC estimation, the different obtained battery models have been paired with an Extended Kalman Filter (EKF) with forgetting factor as introduced for SoC estimation in [20]. Instead of tuning individual process and output covariances, this approach exploits the structure of the overpotential model to be able to use only one tuning parameter, i.e., the forgetting factor. This parameter determines the extent to which the error between measured and predicted output is used to update the state estimate, i.e., a low level of forgetting means stronger reliance on state prediction (which means the SoC predicted through Coulomb counting), whereas stronger forgetting results in larger update steps based on the error between predicted and measured terminal voltage. To judge the quality of the model based on SoC estimation, the forgetting factor is tuned towards the latter, as accurate SoC estimates are linked more strongly to model accuracy. For details on the exact model, identification approach and the exact EKF applied here, the reader is referred to previous work of the authors [27].

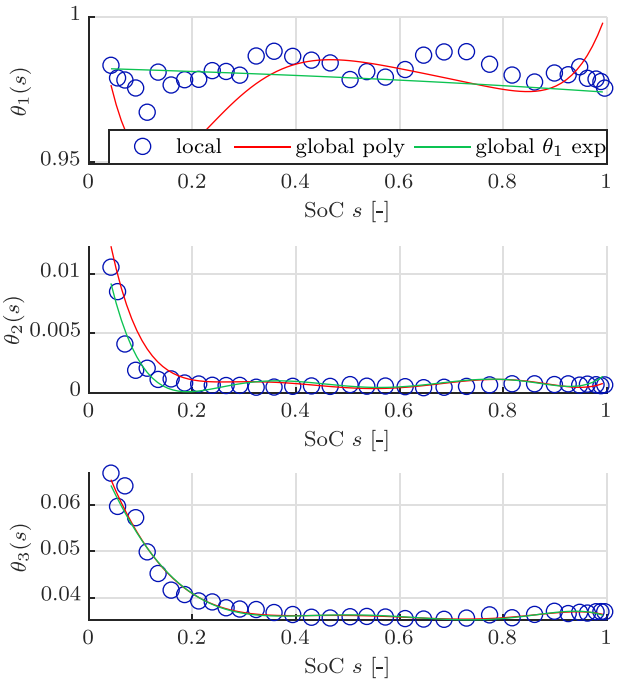

Fig. 4. Example of parametric dependency found through the different approaches for the NMC cell.

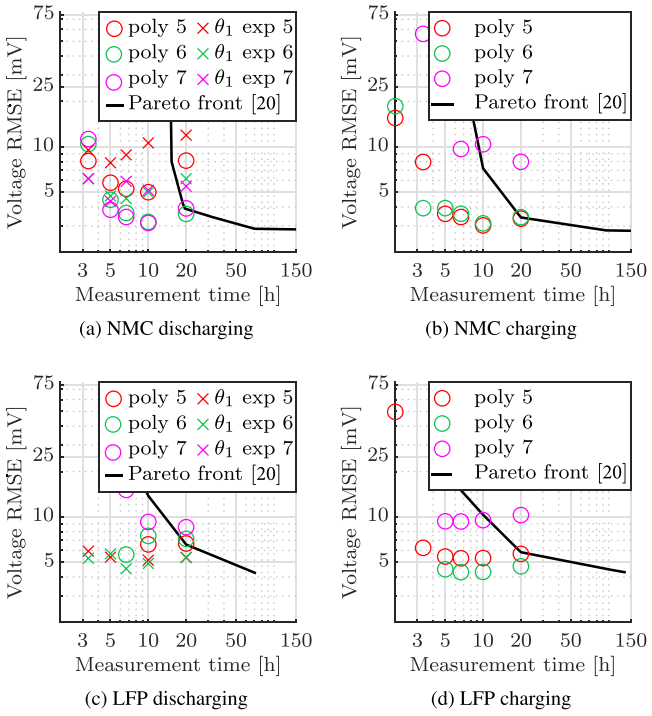

Fig. 5. Relation between voltage prediction error and measurement time required for each EMF.

In terms of results, the relation of required measurement time, and voltage simulation and SoC estimation RMSE achieved on the validation drive cycles by the complete identified models are shown in Figs. 5 and 6. Here, the Pareto-fronts mark the best achieved results, in terms of lowest voltage or SoC estimation RMSEs combined with the shortest required measurement time, obtained in [19], which considered the cascaded approach where first the EMF and then the overpotential model have been identified. Note that the different measurement times at which the results are plotted, directly correspond to the inverse of the associated CC-curve C-rate, e.g., 0.1C corresponds to 10 h of measurement time. Before considering the results in more detail, note that for the discharge model both the polynomial and exponential basis, as in (22), have been employed, while for charging only polynomial basis functions have been used, as there the exponential basis function did not constitute any improvement. Overall, Fig. 5 shows that firstly the results from [19] can be improved significantly, especially in terms of required measurement time, by employing the iterative scheme to essentially upgrade the CC-charge and -discharge curves to accurate EMF models. Secondly, by comparing these results to those in Fig. 3, it has been found that the best results are again achieved by the same polynomial orders for the basis functions. In terms of SoC estimation results in Fig. 6, the results are consistent with those in Fig. 5, i.e., lower voltage RMSE also corresponds to lower SoC estimation RMSE. The only outlier is found in Fig. 5(d), where lower C-rates (higher measurement times) correspond to higher errors instead of vice versa. In this case the retrieved realisation of the EMF fails to accurately capture the slope at high SoC and as a result the EKF also fails to estimate the SoC at this point. The slope is more pronounced for CC-charge curves with a larger C-rate and therefore the accuracy increases as the C-rates increases. Overall, the retrieved errors, with voltage prediction errors in the order of 2 to 5 mV in the SoC range excluding the very low end and SoC estimation errors in the order of 0.2 to 1% SoC, are consistent or slightly better than those retrieved in literature, see, e.g., [8,19,20].

Apart from considering the voltage simulation and SoC estimation errors, the retrieved EMF realisations $g(s)$ itself have also been examined. In Fig. 7, an example of the retrieved EMF realisations corresponding to the 0.1C CC-charge and -discharge curves is shown together with the 0.1C CC-curves used in the iterative scheme and the EMF curves obtained through the extrapolation method in [19]. For both cells, the EMF curves are similar to a large extent. However, the extrapolation-based EMFs are derived from the CC-curves with C-rates $\{0.05, 0.1, 0.15, 0.2\}C$ corresponding to approximately 120 to 140 h of measurement time including intermediate charging or discharging, while the EMFs obtained through the iterative approach only require one CC-(dis)charge curve. Overall, this establishes a measurement time reduction of a factor of 7 to 35 depending on the desired C-rate, thus lowering the overall required experimental efforts to obtain a battery model significantly, while achieving similar accuracy.

4.3. Time-domain showcase

Finally, we want to show the performance that is now achieved by the different presented models in a more intuitive way than only reporting the achieved RMSEs. While this is effective for comparing large quantities of variables, it may not quite convey the level of precision that these models achieve. To do this, we have selected the best realisation for each model type, i.e., corresponding to their lowest voltage RMSE, and we have plotted the predicted voltages on the discharge validation cycle in the time domain together with the measured terminal voltage for both chemistries, as shown in Fig. 8. To put things in perspective, we have also provided the prediction produced by a non-SoC-dependent LTI model which was fitted on identification data spanning an SoC window between 0.5 and 0.95.

Comparing the performance of the different LPV models and the LTI model at the right hand side of Figs. 8(a) and 8(b), it is clear why the SoC dependency needs to be included. However, upon closer inspection, we can see that, although the LPV models significantly increase the accuracy, they still diverge from the measurement at the very end of the cycle, which could be due to nonlinear behaviour encountered in [29]. Nevertheless, the rise in error at low SoC is consistent with errors found in literature, see, e.g., [8]. What is less obvious, but already hinted on by high SoC insets in Fig. 8, is that the

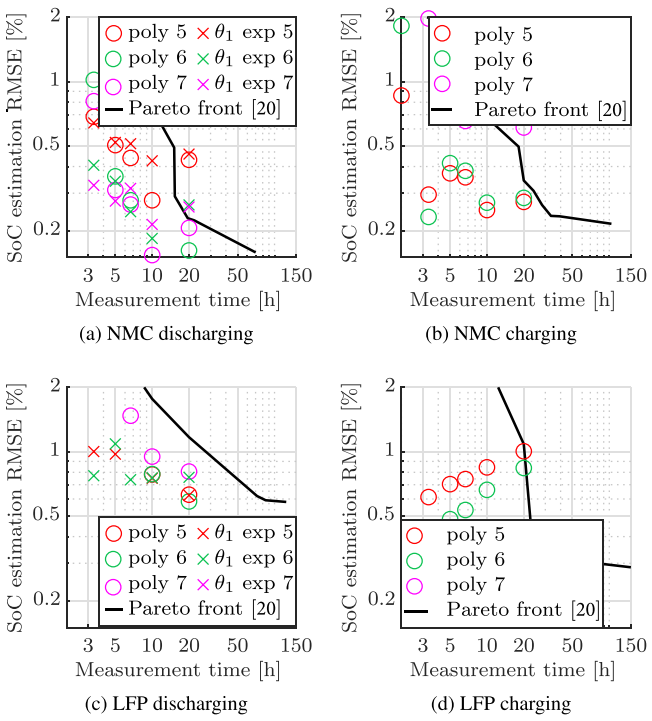

Fig. 6. Relation between SoC estimation error and measurement time required for each EMF.

inclusion of SoC dependency also improves the performance at higher SoC levels. To show this, we have computed the RMSEs achieved by the selected models in the first 10 000 s ($k < 10\,000$ s) and the remaining time ($k > 10\,000$ s) of the cycle and have listed these in Table 1. This shows that a significant reduction in error is achieved by incorporating the SoC dependency for the higher SoC regions, especially when using the local approach. Secondly, the RMSEs corresponding to $k > 10\,000$ s show that the global approach performs better for modelling the stronger dependency at low SoC. To summarise, empirical models are incredibly good at predicting voltage behaviour for batteries and LPV methods allow us to easily capture the required SoC dependencies. Extensions to temperature-dependency have been made in [12].

5. Conclusion

In conclusion, we have developed local and global LPV-IO modelling approaches and proposed an iterative scheme which identifies both the EMF and the overpotential model based on data resulting from short experiments as compared to traditional cascaded approach which requires long experiments, especially for the EMF. By testing the LPV approaches on data gathered from two different cells, we have found that LPV-ARX yields accurate results for both the local and global approach, where the model obtained through the global approach performs slightly better at low SoC. Moreover, by comparing obtained EMF realisations to those obtained through widely used approaches, we have confirmed that the iterative approach yields models with accuracy comparable or slightly better than to those obtained through traditional approaches, but using an EMF experiment which is 7 to 35 times faster. Moreover, the consistency of the results between the two cells provides confidence that this approach will also perform well for other celltypes or chemistries. Overall, the proposed iterative scheme is a cost-effective approach for accurate empirical battery modelling. Since the required data can potentially be gathered during normal use, it could be possible to both initiate and update battery models of battery packs in operation.

Table 1
RMSEs in mV corresponding to the models in Fig. 8.

RMSE (mV)	$k < 10\,000$ s		$k > 10\,000$ s	
	NMC	LFP	NMC	LFP
LTI	4.9	4.6	67	89
local	1.7	2.7	17	25
global poly	3.9	3.1	22	18
global exp	4.0	3.1	17	18
iterative	2.3	3.2	20	26

CRediT authorship contribution statement

F.S.J. Hoekstra: Conceptualisation, Methodology, Software, Validation, Formal analysis, Investigation, Resources, Data curation, Writing – original draft, Visualisation. **M.C.F. Donkers:** Conceptualisation, Methodology, Validation, Formal analysis, Writing – review & editing, Supervision, Funding acquisition. **H.J. Bergveld:** Conceptualisation, Methodology, Validation, Writing – review & editing, Supervision, Funding acquisition.

Declaration of competing interest

The authors declare that they have no known competing financial interests or personal relationships that could have appeared to influence the work reported in this paper.

Data availability

Data will be made available on request.

Acknowledgements

This project has received funding from the European Union's Horizon 2020 research and innovation programme under grant agreement No 957273. The project is part of BATTERY 2030+, the large-scale European research initiative for inventing the sustainable batteries of the future.

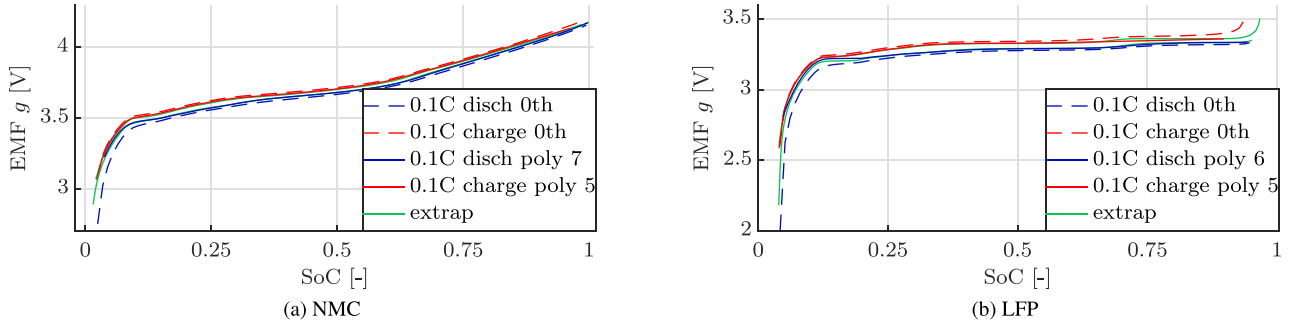

Fig. 7. Example of one of the obtained EMFs compared to EMFs obtained using the extrapolation-based approach applied in [19], where 'extrap' denotes both the charging and discharging EMF.

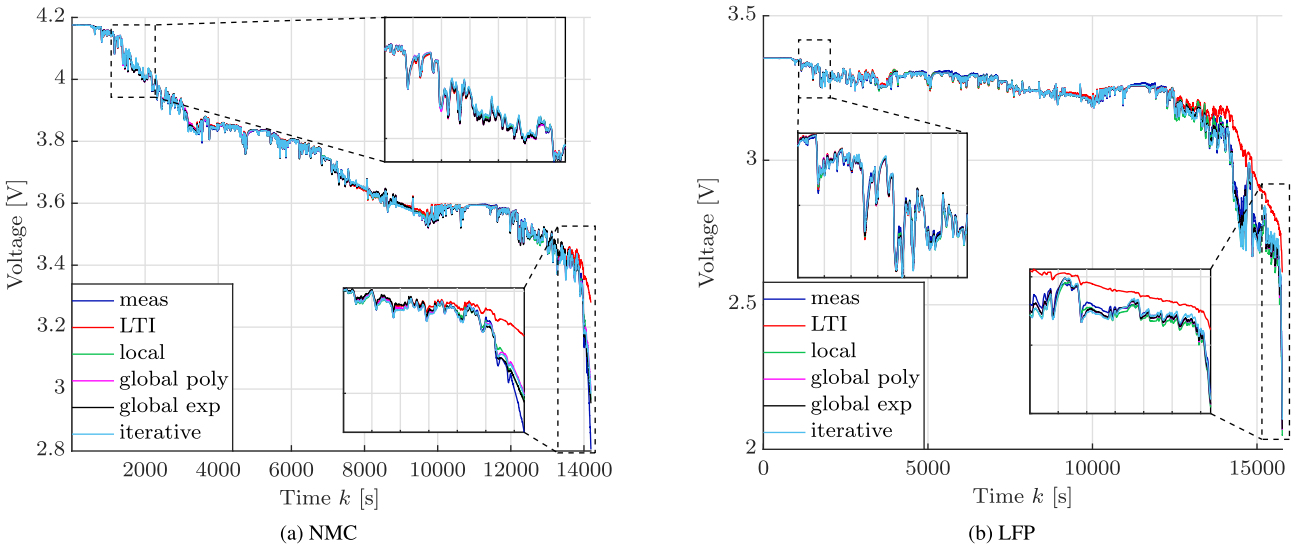

Fig. 8. Time-domain comparison of available models.

References

[1] D.H. Doughty, E.P. Roth, A general discussion of Li ion battery safety, Electrochem. Soc. Interface 21 (2) (2012) 37.

[2] C. Zou, X. Hu, Z. Wei, T. Wik, B. Egardt, Electrochemical estimation and control for lithium-ion battery health-aware fast charging, IEEE Trans. Ind. Electron. 65 (8) (2017) 6635–6645.

[3] H.E. Perez, X. Hu, S.J. Moura, Optimal charging of batteries via a single particle model with electrolyte and thermal dynamics, in: Proceedings of the IEEE American Control Conference, 2016, pp. 4000–4005.

[4] M. Debert, G. Colin, G. Bloch, Y. Chamaillard, An observer looks at the cell temperature in automotive battery packs, Control Eng. Pract. 21 (8) (2013) 1035–1042.

[5] M. Einhorn, F.V. Conte, C. Kral, J. Fleig, Comparison, selection, and parameterization of electrical battery models for automotive applications, IEEE Trans. Power Electron. 28 (3) (2012) 1429–1437.

[6] C. Zhang, K. Li, S. Mcloone, Z. Yang, Battery modelling methods for electric vehicles-A review, in: Proceedings of the IEEE European Control Conference, 2014, pp. 2673–2678.

[7] D. Andre, M. Meiler, K. Steiner, H. Walz, T. Soczka-Guth, D. Sauer, Characterization of high-power lithium-ion batteries by electrochemical impedance spectroscopy. II: Modelling, J. Power Sources 196 (12) (2011) 5349–5356.

[8] P. Schröer, E. Khoshbakht, T. Nemeth, M. Kuipers, H. Zappen, D.U. Sauer, Adaptive modeling in the frequency and time domain of high-power lithium titanate oxide cells in battery management systems, J. Energy Storage 32 (2020) 101966.

[9] X. Lin, H.E. Perez, S. Mohan, J.B. Siegel, A.G. Stefanopoulou, Y. Ding, M.P. Castanier, A lumped-parameter electro-thermal model for cylindrical batteries, J. Power Sources 257 (2014) 1–11.

[10] C.R. Birkl, D.A. Howey, Model identification and parameter estimation for LiFePO4 batteries, in: Proceedings of the IET Hybrid and Electric Vehicles Conference, 2013.

[11] R. Tóth, Modeling and Identification of Linear Parameter-Varying Systems, Vol. 403, Springer, 2010.

[12] F.S.J. Hoekstra, Y.J.J. Heuts, H.J. Bergveld, M.C.F. Donkers, Empirical battery modelling for high currents: The effect of nonlinear overpotential and inevitable self-heating, IFAC-PapersOnLine 53 (2) (2020) 12440–12445.

[13] A. Bachnas, R. Tóth, J. Ludlage, A. Mesbah, A review on data-driven linear parameter-varying modeling approaches: A high-purity distillation column case study, J. Process Control 24 (4) (2014) 272–285.

[14] P.B. Cox, Towards Efficient Identification of Linear Parameter-Varying State-Space Models (Ph.D. thesis), Eindhoven University of Technology, 2018.

[15] J.-W. Van Wingerden, M. Verhaegen, Subspace identification of bilinear and LPV systems for open-and closed-loop data, Automatica 45 (2) (2009) 372–381.

[16] Y. Hu, S. Yurkovich, Y. Guezennec, R. Bornatico, Model-based calibration for battery characterization in HEV applications, in: Proceedings of the IEEE American Control Conference, 2008, pp. 318–325.

[17] Y. Hu, S. Yurkovich, Y. Guezennec, B. Yurkovich, A technique for dynamic battery model identification in automotive applications using linear parameter varying structures, Control Eng. Pract. 17 (10) (2009) 1190–1201.

[18] Y. Li, J. Yang, W. Liu, L. Wang, C. Liao, Linear parameter-varying modeling and identification of lithium-ion battery for control-oriented applications, J. Power Sources 507 (2021) 230304.

[19] F.S.J. Hoekstra, L.H.J. Raijmakers, M.C.F. Donkers, H.J. Bergveld, Comparison of battery electromotive-force measurement and modelling approaches, J. Energy Storage 56 (2022) 105910.

[20] H. Beelen, H.J. Bergveld, M.C.F. Donkers, Joint estimation of battery parameters and state of charge using an extended Kalman filter: a single-parameter tuning approach, IEEE Trans. Control Syst. Technol. 29 (3) (2020) 1087–1101.

[21] Y. Hu, S. Yurkovich, Linear parameter varying battery model identification using subspace methods, J. Power Sources 196 (5) (2011) 2913–2923.

[22] Y. Zhao, B. Huang, H. Su, J. Chu, Prediction error method for identification of LPV models, J. Process Control 22 (1) (2012) 180–193.

[23] C. Hoffmann, H. Werner, A survey of linear parameter-varying control applications validated by experiments or high-fidelity simulations, IEEE Trans. Control Syst. Technol. 23 (2) (2014) 416–433.

[24] L. Ljung, System Identification: Theory for the User, Prentice Hall, 1987.

[25] R. Tóth, H.S. Abbas, H. Werner, On the state-space realization of LPV input-output models: Practical approaches, IEEE Trans. Control Syst. Technol. 20 (1) (2012) 139–153.

[26] P. den Boef, P.B. Cox, R. Tóth, Lpvcore: MATLAB toolbox for LPV modelling, identification and control, IFAC-PapersOnLine 54 (7) (2021) 385–390.

[27] F.S.J. Hoekstra, H.J. Bergveld, M.C.F. Donkers, Towards state-of-charge estimation for battery packs: Reducing computational complexity by optimising model sampling time and update frequency of the extended Kalman filter, in: Proceedings of the IEEE American Control Conference, 2021, pp. 3120–3125.

[28] H.P.G.J. Beelen, H.J. Bergveld, M.C.F. Donkers, On experiment design for parameter estimation of equivalent-circuit battery models, in: 2018 IEEE Conference on Control Technology and Applications (CCTA), pp. 1526–1531.

[29] R. Relan, Y. Firouz, J.-M. Timmermans, J. Schoukens, Data-driven nonlinear identification of Li-ion battery based on a frequency domain nonparametric analysis, IEEE Trans. Control Syst. Technol. 25 (5) (2016) 1825–1832.

[30] Y. Wang, H. Fang, L. Zhou, T. Wada, Revisiting the state-of-charge estimation for lithium-ion batteries: A methodical investigation of the extended Kalman filter approach, IEEE Control Syst. Mag. 37 (4) (2017) 73–96.